Rapid transition from continental breakup to ocean crust at South China Sea rifted margin

H. C. Larsen[a*], G. Mohn[b*], M. Nirrengarten[b], Z. Sun[c], J. Stock[d], Z. Jian[e], C. Alvarez-Zarikian[f], J. Boaga[g], S.A. Bowden[h], A. Briais[i], Y. Chen[j], D. Cukur[k], K. Dadd[l], W. Ding[m], M. Dorais[n], E. Ferre[o], F. Ferreira[p], A. Furusawa[q], A. Gewecke[r], J. Hinojosa[d], T. Hoefig[f], K. Hsiung[s], B. Huang[t], E. Huang[e], X. Huang[u], S. Jiang[v], H. Jin[t], B. Johnson[w], A. Klaus[f], R. Kurzawski[x], C. Lei[y], B. Li[z], L. Li[e], Y. Li[aa], J. Lin[ab], C. Liu[ac], C. Liu[e], Z. Liu[e], A. Luna[ad], C. Lupi[ae], A. McCarthy[af], L. Ningthoujam[ag], , N. Osono[ah], D. Peate[ai], P. Persaud[ac], N. Qiu[c], C. Robinson[aj], S. Satolli[ak], I. Sauermilch[al], J. Schindlbeck[x], S. Skinner[am], S. Straub[an], X. Su[c], C. Su[ao], L. Tian[ap], F. van der Zwan[aq], S. Wan[ar], H. Wu[as], R. Xiang[c], R. Yadav[ag], L. Yi[e], P., C. Zhang[c], J. Zhang[c], Y. Zhang[at], N. Zhao[ab], G. Zhong[e], L. Zhong[au]

[a] School of Ocean and Earth Science, Tongji University, 1239 Siping Road, Shanghai 200092, China

[b] Laboratoire Géosciences et Environnement Cergy (GEC), Maison Internationale de la Recherche, Université de Cergy-Pontoise, 1, rue Descartes, 95000 Neuville-sur-Oise, France

*Corresponding Authors. hclarseniodp@gmail.com, geoffroy.mohn@u-cergy.fr

Magmatism at rifted margins shows widely different developments: margins with transient, abundant magmatism (magma-rich), and magma-poor margins. Magma-poor margins, as exemplified by the North Atlantic Iberia-Newfoundland margin (INFM), are accompanied by extreme crustal thinning and mantle exhumation across wide (~100 km) zones prior to the formation of igneous oceanic crust. The discovery of the structure of the INFM caused a paradigm change and has been invoked to interpret seismic imaging across many other rifted margins, including the northern South China Sea (SCS) margin. International Ocean Discovery Program (IODP) expeditions 367/368 to the northern SCS, for the first time, tested the INFM model on a different rifted margin through drilling. Contrary to the INFM model, results from the highly extended SCS margin show initiation of MORB-type basaltic magmatism during final breakup, and rapid transition into formation of normal thickness oceanic crust. Cores suggests that crustal extension was fast, and no evidence of mantle exhumation was

recovered by drilling. Major and rapid crustal thinning within a relatively thin pre-rift lithosphere may have caused early melts to weaken the lithosphere, and allowed asthenospheric upwelling at rates sufficient to generate the observed magmatism by decompression melting of normal temperature mantle.

The well surveyed northern South China Sea (SCS) margin (Fig. 1) offers an opportunity for comparison with the two end members identified by North Atlantic drilling[1,2]: magma-rich and magma-poor margins[3]. The SCS margin features none of the characteristics of the truly magma-rich margins [4] such as transient formation of excessively thick igneous crust (15-30km) and 5+ km thick seaward-dipping reflectors [5,6]. On the contrary, its structural architecture is reminiscent of the highly extended and magma-poor Iberia-Newfoundland Margin (INFM)[7–10] . However, the SCS formed within younger lithosphere, exhibits higher rate of initial ocean seafloor spreading [11] than the INFM, and therefore provides for different geodynamic boundary conditions. Intriguingly, this IODP margin study reveals the first well-established example of the 'missing link' between volcanic rifted margins and magma-poor, hyperextended margins, and thus raises fundamental geodynamic questions about the mechanisms of continental breakup and plate separation.

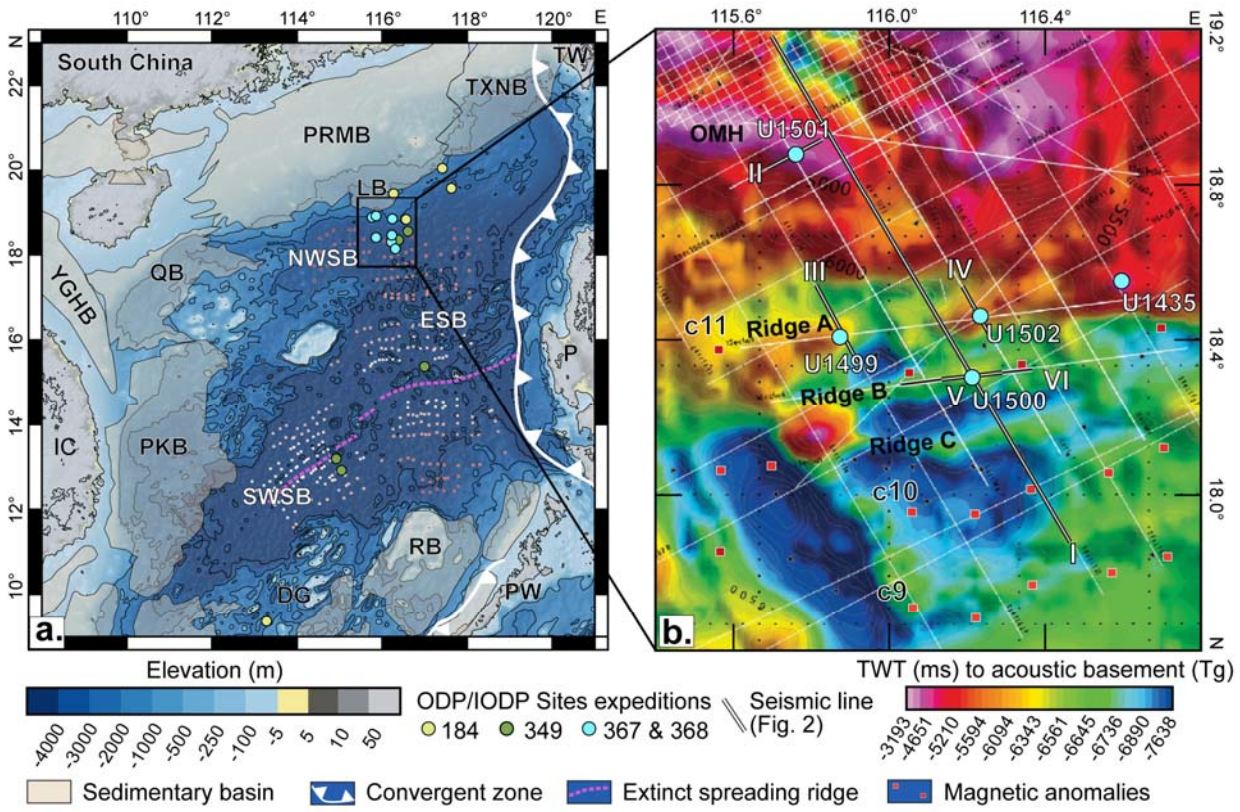

Figure 1: a. Topographic map of the SCS[31] with the location of IODP/ODP Sites[14,32,33]. b. Depth to acoustic basement and regional seismic dataset modified from[17]. Bold white lines refer to seismic data in Figure 2. Magnetic anomalies[13,34]. Sedimentary basins: Pearl River Mouth Basin (PRMD), Liwan Basin (LB), Qiongdongnan Basin (QB), Phu Khanh Basin (PKB), Reed Bank (RB), Taxinan Basin (TXNB). Ocean sub-basins: Eastern sub-basin (ESB), North West sub-basin (NWSB), South West Sub-Basin (SWSB). IC: Indochina, PW: Palawan, P: Philippines, TW: Taiwan. DG: Dangerous Ground

Tectonic setting of the SCS basin

The SCS oceanic basin formed during the early Oligocene to middle Miocene (32-15 Ma)[12–14]. Its development includes several sub-basins (Fig. 1a) and rift propagation events[14]. Our study focus on a ~ 100 km long margin segment at the northern SCS margin within the north-west sub-basin (Fig. 1a) stretching seawards from the deep Liwan Basin to oceanic crust (Figs. 1 and 2I). Previous studies suggest that the main rifting is of Eocene age with final breakup during the early Oligocene[14,15]. The margin structure has been interpreted as highly extended and magma-

poor, possibly hosting exhumed lower crust and mantle in its distal parts[16,17], to show a delay between final breakup and onset of major igneous activity, and later overprinted by the late Miocene Hainan plume[18].

The oldest magnetic anomaly interpreted to be present along the studied margin segment is C11n (~29.5 Ma; early Oligocene) (Fig. 1[13]), but it has low amplitude suggesting other mechanisms [19] than seafloor spreading could be invoked to explain it. Younger magnetic anomalies within the SCS basin are stronger, and mature oceanic crust of normal thickness and mid-ocean ridge basalt (MORB) composition is verified by drilling[14]. Initial seafloor spreading was lower end of intermediate (half-rate: 2.5 cm/yr)[11,13].

A deep crustal reflection seismic profile from the regional 2D seismic lines (Fig. 1) interpreted prior to drilling is shown in Figure 2I. The basement of the Liwan Basin is characterized by highly thinned crust, 10 km or less thick, where the upper to mid crust has undergone extensive normal faulting, and the development of thick (up to 6–8 km) rift basins[20] (Fig. 2I). Post-rift fill attains thicknesses of 2 km or locally more. Most of the extensional faults appear to root into a major decollement at mid- to lower-crustal levels. The Liwan Basin is bounded seaward by the Outer Margin High (OMH). Crustal thickness decreases markedly seaward of the OMH. The main decollement level is interpreted to continue laterally seawards below the OMH. Unlike the Moho reflection, which remains strong until a crustal thickness of 6-8 km is reached within the distal margin (Ridge A of Fig. 1 and 2), the faults at the base of the OMH cannot be followed with confidence this far (Fig. 2). The lower crust shows variable thickness, thinnest (~8 km) below the deep rift basins, yet it thickens below the OMH, suggesting that the lower crust remained ductile and able to flow during rifting[21–23].

Drilling results and linkage to seismic data

IODP Site U1501 was drilled on the crest of the OMH (Figs. 2I and 2II), and successfully penetrated acoustic basement (Tg) below syn- and post-rift sediments (Fig. 3). Two distinct lithostratigraphic units, separated by an unconformity (T60; ~26 Ma), were recovered above

reflector Tg: (1) a mixed succession of upper Miocene to Pleistocene calcareous-rich sediment and calcareous ooze; and (2) a succession of lowermost Oligocene and possibly upper Eocene siliciclastic sediment. The lower unit is ~300 m thick and shows a record of continuous and uniform sedimentation with a trend of upward fining beds dipping ~5 degrees northeast. The base of the succession contains coarse sand intervals with up to pebble-sized clasts that are interbedded with mm thin beds of lignite or coal and glauconite-bearing sand. Throughout the uppermost ~80 m of the succession, the coarse sand transitions into fine sand, silt and clay. This change is accompanied by the presence of lower Oligocene microfossils, suggesting that the basin underwent deepening and starved in clastic input from the Eocene–Oligocene boundary (ca. 34 Ma). Deepening of the basin within this time interval is consistent with the inferred ca. 32–30 Ma age of final breakup along the northern SCS[11,14], but is not associated with any unconformity in either seismic data or the drill cores (Fig. 3). Nevertheless, we infer that this succession of early Oligocene–Eocene sediments corresponds to syn-rift deposition along the northern margin of the SCS. Site U1435[14] (Fig. 1) recovered similar facies and age syn-rift sediments.

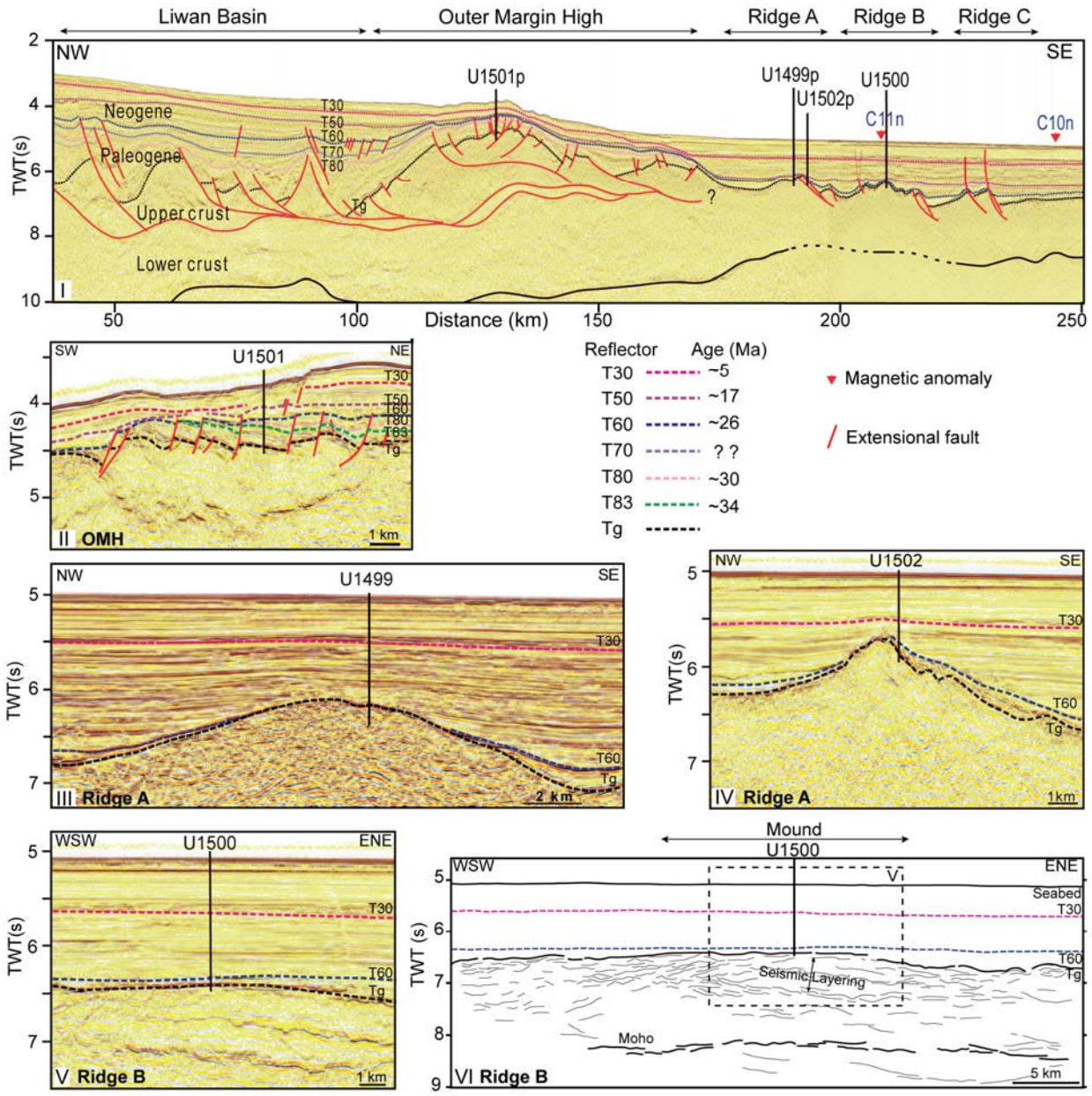

Figure 2: Interpreted seismic sections (location in Figure 1). Drill sites marked with 'p' are projected into the main cross-line. Regional seismic stratigraphic unconformities T30-T83 with ages obtained from IODP drill cores. T70 was not sampled. Tg: Acoustic basement. Sub Tg stratigraphic relationships can be locally interpreted. Lithologies sub-cropping below Tg ranges from Oligocene syn-rift sediments, through Oligocene submarine basalts to pre-rift sediments (Mesozoic?); see Figure 3. Black line: Moho reflector, location below Site U1500 from cross-line in panel VI. Seimics data courtesy of Chinese National Offshore Oil and Gas Company (CNOOC).

The boundary (Tg) between the syn-rift succession and the underlying formation at Site U1501 is a positive, high-amplitude seismic reflector (Figs. 2II, 3). The seismic data (Fig. 2II) indicates the presence of tilted and locally folded beds below Tg, and drill cores recovered highly lithified, ~20-degree dipping, coarse sandstones to conglomerates (Fig. 3). Their dip, degree of lithification, and a sudden downward increase in seismic velocities and density measured on the cores suggest that these sediments underwent an earlier deformational event prior to Eocene rifting.

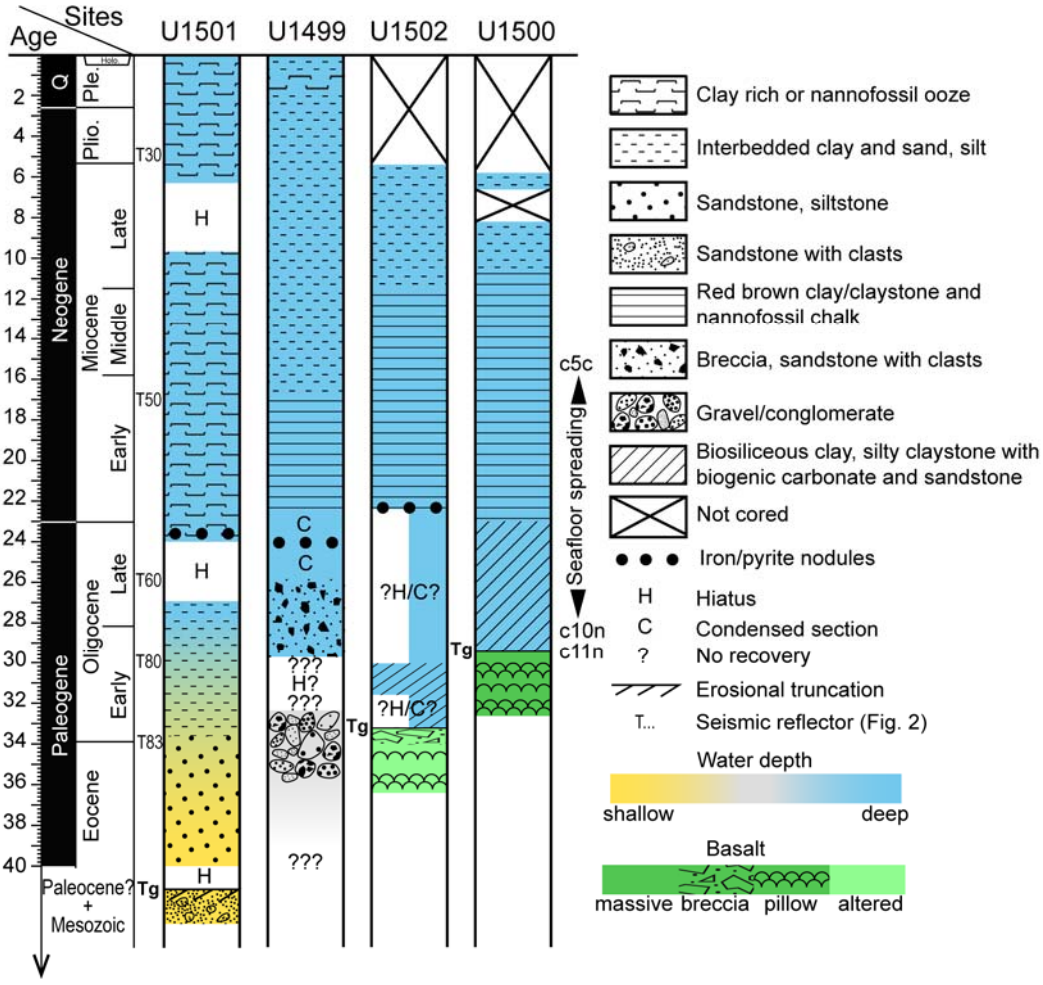

Figure 3: Summary chart of drilling results. All details and background material are in the IODP 367-368 Proceeding volume [33]

Seaward of the OMH, three distinct linear ridges - Ridges A, B and C (Figs. 1B and 2) - parallel the margin, trending from west-southwest to east-northeast. The extensional faults bounding ridges B and C are extremely uniform along strike for ~100 km, and the top of the basement reflection along these two ridges is remarkably continuous and flat (Fig. 2V, VI). Seismic reflections showing clear layering below Tg are seen on both ridges, and can in places be followed to significant depths (Ridge B; ~ 2km) (Fig. 2V and VI). Magnetic anomaly C11n is located close to Ridge B and C10n seaward of Ridge C (Figs 1 and 2). Contrary to ridges B and C, Ridge A shows significant morphological variation (depth, width, reflection character) along strike. The seismic reflections below Tg do not form any regional systematic pattern that can be interpreted with confidence (Fig. 2). The continental Moho reflector below the OMH can be followed seawards to, but not below Ridge A (Fig. 2). A less clear Moho reflector re-appears below Ridge B and C (Fig. 2I, VI), and continues further seawards below the oceanic crust.

IODP Sites U1499 and U1502 sampled Ridge A (Figs. 2I, II, III and 3), but yielded widely different results consistent with their different seismic images. The lower intervals of Site U1499 consists of a condensed succession of lowermost Miocene and upper Oligocene fine-grained red clay, with strongly lithified red claystone at the base of the succession. Below the red clay, the cored intervals recovered coarse siliciclastic sediments (top to bottom) composed of a matrix supported breccia of sand with angular and pebble-sized sedimentary clasts, followed downwards by a succession of very coarse-grained gravel, mostly consisting of cobble-sized clasts. The clasts within the gravel predominantly comprise previously eroded sedimentary rocks (mostly coarse-grained sandstone). The age of the gravel unit is tentatively constrained by the presence of upper Oligocene clays above, and a single, lower Oligocene age datum within the unit itself.

Site U1502 is located 40 km to the east along Ridge A (Fig. 2III). The Tg here forms an onlapping surface and is characterized by a set of strong, parallel and dipping (~25^{o}) reflectors below which no coherent seismic energy can be seen. A total of 180 m of basaltic lavas with pillow structures representing the acoustic basement were recovered, overlain by a sequence of

deep-marine, upper Oligocene to lower Miocene sediments (Fig. 3). No significant amount of sediments was observed between the lavas suggesting rapid emplacement of the flows. The basalt flows suffered pervasive hydrothermal alteration up to greenschist facies conditions and profound brecciation (hydro-fracturing) associated with massive iron-sulphide mineralization. The effect of strong hydrothermal activity (with minor brecciation), extends ~5 metres into the overlying, deep-marine sediments of Oligocene age (Fig.3). Given the basaltic nature of the lavas, the original depositional dip is inferred to be only a few degrees. The seismic image of the overlying sedimentary section does not show significant tilting of these, and hence, volcanism, seaward tilting of the fault-block and hydrothermal activity is confined to a brief period of time.

Seismic data (Fig. 2) suggests that Ridge A is floored, at least partially, by continental crust, and coring captured the interplay between extensional basin development stage and magmatism. The sandstone and gravels recovered from the base of Site U1499 possibly were deposited by submarine gravity flows in response to late-stage rifting of the northern SCS. The basalt flows recovered at Site U1502 within the more easterly part of Ridge A record syn-rift magmatism that occurred in conjunction with the rift-to-drift transition of the SCS. This magmatism is not seen at Site U1499 and may not have continued southwest-ward from Site U1502 all along the ridge A.

Site U1500 on Ridge B cored through 1380 m of deep marine Neogene to late Paleogene sediments and recovered 150 m of volcanic basement below Tg (Fig. 2I, V). Basement consists of fresh basaltic flows alternating between thick massive flows and pillow flows (Fig. 3). The inferred Oligocene age of cm-thin, clayish marine sediments intercalated within the upper lavas is consistent with both the presence of deep-marine, upper Oligocene to lower Miocene sediments deposited on the igneous basement, and the proximity (Figs 2 and 3) of magnetic chron C11n (early Oligocene, ca. 29.5 Ma). The seismic strike-line (Fig. 2V, VI) shows that the basement cored at Site U1500 is acoustically layered down to ~ 2 km below Tg (Vp of 4.5 – 5.0 km/s measured at the drill core). This deep seismic layering is also observed along a wider section of the line (Fig. 2VI), revealing that Site U1500 is located at the crest of a mound-like

structure overlain by younger strata towards the southwest. This stratigraphic pattern is interpreted to reflect time-wise migration of the centre of extrusive activity southwest-wards along the rift axis. This development is equally consistent with an advanced stage of rifting as well as full ocean floor spreading, but importantly, either of the two cases is proof that considerable, MORB type magmatism along the entire Ridge B was established by Chron C11n time. Ridge C is associated with the well-developed spreading anomaly C10r and forms, apart from its fault-bounded nature, a straight continuation into the younger SCS ocean crust[11,14].

The key for understanding the morphological evolution of ridges B and C is that they only developed as ridges after magmatism. They are both landwards tilted fault blocks bounded by seaward-dipping normal faults (Fig. 2). Along strike, the top of Ridge B and C are remarkably flat, non-faulted and continuous for ~ 100 km, implying that the seaward-dipping normal faults are ridge parallel and laterally very extensive. The normal faults show significant displacements (up to ~ 500 m) of the igneous basement, but do not affect the overlying latest Oligocene to early Miocene sediments. Faulting thus occurrence within a short mid-Oligocene time interval. Faulting at a similar scale is not seen seaward of Ridge C (Fig. 2I) suggesting this tectonic activity was a transient process during the breakup to early seafloor spreading interval.

Importantly, the composition of the basalts from ridges A and B forms a continuum with that of the igneous ocean crust sampled by IODP Expedition 349 within the younger SCS basin[14]. Site U1500 and U1502 lavas all have MORB compositions (Fig. 4) with MORB-like petrography (highly plagioclase phyric, olivine-bearing, lacking clinopyroxene phenocrysts). This is consistent with mantle-derived primitive, dry melts, generated by decompression melting in a mid-ocean-ridge setting. From this, we infer that a melting regime comparable to a mature spreading centre in terms of melt composition, productivity and lateral extent was present during final breakup.

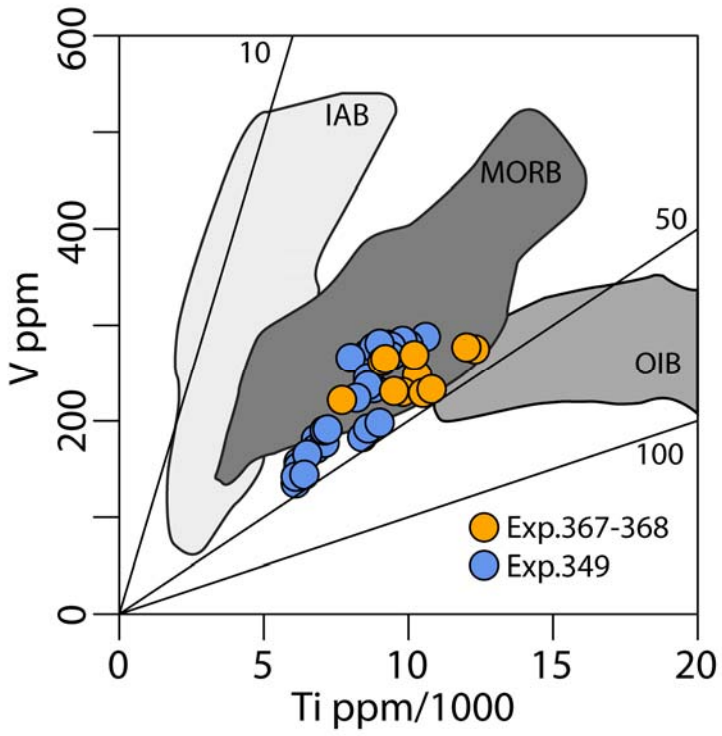

Figure 4: Ti-V discrimination diagram[35] of basalts sampled by IODP expeditions 367-368 (margin Sites U1500 and 1502)[33] and IODP 349 sites located on oceanic crust[14]. (See supplementary material)

Discussion and conclusion

Our unique drilling data supports the kinematic history of the SCS with breakup during the Oligocene at around magnetic chron C11n (~30 Ma), but questions previous interpretations of mantle exhumation and initial magma starvation[16,17]. Whether full igneous ocean crust formed right from the beginning of plate separation around C11n time, or a transitional crust (Fig. 5) with a large component of igneous material formed during a brief period (~ 1 myr) from ~C11n and into C10r cannot be resolved by current geophysical and geochemical data. This uncertainty, however, has only negligible impact on the requirement for a mature, productive mantle melting regime to be in place no later than ~30 Ma. The potentially slightly older basalts at Ridge A (U1502 in Fig. 3) likely a less extensive along the rift than Ridge B extrusive, but nevertheless share the same bulk composition, suggesting a similar melting regime.

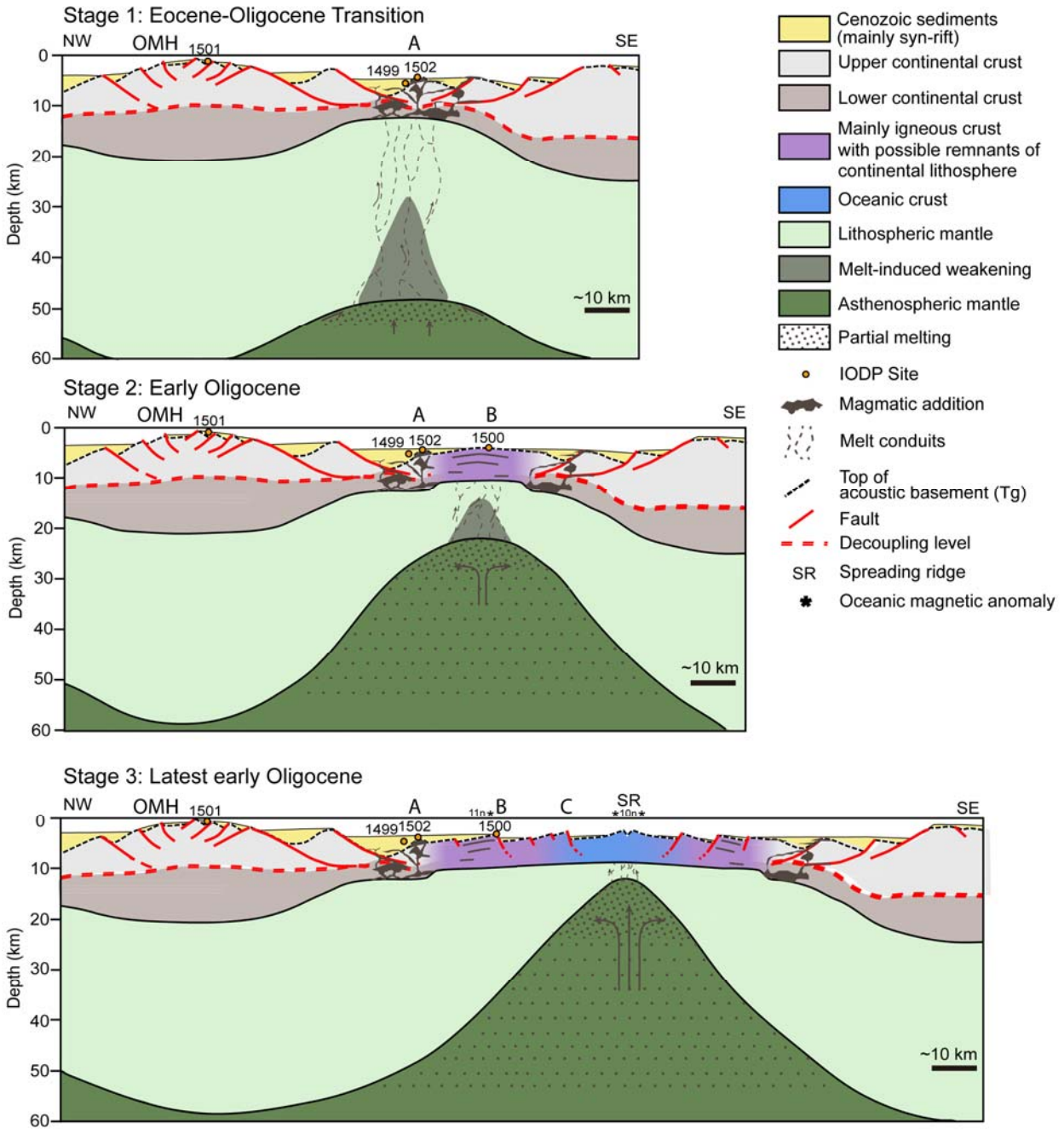

Figure 5: Conceptual model of three stages of breakup based on integration of seismic and drilling data (Figs. 2, 3). Stage 1: a deep basin with thin crust existed within final zone of plate rupture and hosted magmatism at 32 – 30 Ma. Initial magmatism (U1502) likely was confined to select parts of the rift zone. Stage 2: Ascending melts rapidly weakened the mantle lithosphere and massive extrusive activity along the entire rift zone takes place, underpinned by a thicker zone of melting in the asthenosphere. Stage 3: Mature seafloor spreading and passive

upwelling of asthenospheric mantle is established. Note that in time, stages 2 and 3 are only ~ 1 myrs apart (or less), but high rate (~ 2.5 cm/yr, half-rate) of plate separation translates to significant distance in space.

At magma-poor margins like the INFM, thinning of crust and the lithospheric mantle is believed to be coupled and primarily driven by faulting and associated mechanical stretching[24]. Magma starvation is explained by slow ascent rates of the asthenosphere constrained by rate of plate separation and the nature of breakup process[25,26]. At volcanic margins, the coincidence of transient, excessive magmatism and breakup is readily explained by emplacement of anomalously hot asthenosphere that provides a mechanism for thermal erosion of the sub-continental lithospheric mantle[27,28]. The uniqueness of the SCS margin is that none of the characteristics of the magma-poor INFM or volcanic margins are present, and therefore its formation requires a rifting model to explain the characteristics of the SCS margin without generating features of the other two types of margins.

We propose a model to illuminate the formation of the SCS margin that is consistent with key crustal observations and involves a plausible mechanism to thin the lithospheric mantle (Fig. 5). The model includes a major and brief period of extension starting in the Eocene before the oldest identified age datum (34 Ma) obtained from the syn-rift fill ~200 m above the basal angular unconformity (Tg) at Site U1501 (Fig. 3). It ended at ~ 30 Ma, and may therefore have been very short-lived. Faulting did not cross through the lower crust, which remained ductile throughout, allowing decoupled extension of crust and mantle to take place across most of the margin. At the extreme distal margin, however, crustal thinning was at a maximum, and seismic data cannot exclude the possibility that faults reached the mantle and that modest amounts of mantle exhumation might have taken place around ridges A to B.

Prior to break up around the Eocene–Oligocene boundary (stage 1 in Fig. 5), continental crust was thinned to ~ 8 km or less. The thickness of the lithosphere likely was smaller than the present day 80 km below southeast China[29] , implying that a 20-25 km of crustal thinning proportion-wise represents major thinning of the entire lithosphere. Discarding effect of any

tectonic stretching of the mantle lithosphere at the location of final breakup, this thinning would allow the asthenosphere to ascend through approximately 1/4 - 1/3 of the window of decompression melting. Provided efficient melting conditions, this could result in a melt column ~1/3 of oceanic crust (i.e., 1-2 km thick), being even more if a gradient driven lateral flow along the lithosphere-asthenosphere boundary took place (Fig. 5). Since melts rise orders of magnitude faster than the solid mantle[27], they can rapidly transfer heat into the overlying lithosphere. However, for this mechanism to work, the ascent rate of asthenospheric mantle should be >1 cm/yr to support effective decompression melting of normal temperature mantle[30]. Rapid rifting and crustal extension is supported by this study, and by the comparatively high initial spreading rates derived from plate kinematic studies(half-rate: 2.5 cm/yr or higher[11,13]. If rate of extension increased linearly from zero to the rate of initial plate separation, passive upwelling rate exceeding 1 cm/yr would be in place within less than half of the rift duration and might enable melt-driven weakening of the lithosphere (stage 1-2 of fig. 5) and eventually final breakup (stage 3 of fig. 5).

A key driver in this model thus is major and fast rifting. Furthermore, the southeast Asia lithosphere has been interpreted as hot and weak[21,23], and potentially susceptible to thinning by melt impregnation. Continued ductility of the lower crust enabled decoupling of crust and mantle extension, and may have been aided by massive sedimentation from the nearby large continent, helping to keep the lower crust hot across most of the margin. It can therefore be hypothesized that it requires specific geodynamic boundary conditions for this type of rifted margin to develop.

Acknowledgement: We are indebted the Chinese National Offshore Oil and Gas Company to provide access for Z.S. and H.C.L. to work on their large regional database of seismic reflection data, which they amended with new data to document our selected drill sites. IODP-China office supported international workshops to develop the original drilling proposal.

References:

1. Lundin, E. R. & Dore, a. G. Hyperextension, serpentinization, and weakening: A new paradigm for rifted margin compressional deformation. *Geology* **39,** 347–350 (2011).
2. Peron-Pinvidic, G., Manatschal, G. & Osmundsen, P. T. Structural comparison of archetypal Atlantic rifted margins: A review of observations and concepts. *Mar. Pet. Geol.* **43,** 21–47 (2013).
3. Franke, D. Rifting, lithosphere breakup and volcanism: Comparison of magma-poor and volcanic rifted margins. *Mar. Pet. Geol.* **43,** 63–87 (2013).
4. Lester, R. *et al.* Rifting and magmatism in the northeastern South China Sea from wide-angle tomography and seismic reflection imaging. *J. Geophys. Res. Solid Earth* **119,** 2305–2323 (2014).
5. Larsen, H. C. & Saunders, A. D. in *Proceedings of the Ocean Drilling Program, 152 Scientific Results* (Ocean Drilling Program, 1998). doi:10.2973/odp.proc.sr.152.240.1998
6. Holbrook, W. S. *et al.* Mantle thermal structure and active upwelling during continental breakup in the North Atlantic. *Earth Planet. Sci. Lett.* **190,** 251–266 (2001).
7. Boillot, G., Winterer, E. L. & Al., E. *Proceedings of the Ocean Drilling Program, 103 Scientific Results*. **103,** (Ocean Drilling Program, 1988).
8. Sawyer, D. S. *Proceedings of the Ocean Drilling Program, 149 Initial Reports*. **149,** (Ocean Drilling Program, 1994).
9. Whitmarsh, R. B., Beslier, M.-O. & Wallace, P. J. *Proceedings of the Ocean Drilling Program, 173 Initial Reports*. **173,** (Ocean Drilling Program, 1998).
10. Tucholke, B. E. & Sibuet, J.-C. *Proceedings of the Ocean Drilling Program, 210 Scientific Results*. **210,** (Ocean Drilling Program, 2006).
11. Li, C.-F. *et al.* Ages and magnetic structures of the South China Sea constrained by deep tow magnetic surveys and IODP Expedition 349. *Geochemistry, Geophys. Geosystems* **15,** 4958–4983 (2014).
12. Taylor, B. & Hayes, D. Origin and history of the South China Sea basin. *Tecton. Geol. Evol.* **27,** (1983).
13. Briais, A., Patriat, P. & Tapponnier, P. Updated interpretation of magnetic anomalies and

seafloor spreading stages in the south China Sea: Implications for the Tertiary tectonics of Southeast Asia. *J. Geophys. Res.* **98,** 6299 (1993).

14. Li, C.-F. *et al.* Proceedings of the International Ocean Discovery Program: Expedition 349 scientific in (2015). doi:10.14379/iodp.proc.349.101.2015

15. Zhou, D., Ru, K. & Chen, H. Kinematics of Cenozoic extension on the South China Sea continental margin and its implications for the tectonic evolution of the region. *Tectonophysics* **251,** 161–177 (1995).

16. Franke, D. *et al.* The final rifting evolution in the South China Sea. *Mar. Pet. Geol.* **58,** 704–720 (2014).

17. Sun, Z. *et al. International Ocean Discovery Program; Expeditions 367 and 368 scientific prospectus; South China Sea rifted margin; testing hypotheses for lithosphere thinning during continental breakup; drilling at the South China Sea rifted margin*. (International Ocean Discovery Program, 2016). doi:10.14379/iodp.sp.367368.2016

18. Fan, C. *et al.* New insights into the magmatism in the northern margin of the South China Sea: Spatial features and volume of intraplate seamounts. *Geochemistry, Geophys. Geosystems* **18,** 2216–2239 (2017).

19. Bronner, A., Sauter, D., Manatschal, G., Péron-Pinvidic, G. & Munschy, M. Magmatic breakup as an explanation for magnetic anomalies at magma-poor rifted margins. *Nat. Geosci.* **4,** 549–553 (2011).

20. Gao, J. *et al.* The continent–ocean transition at the mid-northern margin of the South China Sea. *Tectonophysics* **654,** 1–19 (2015).

21. Clift, P., Lin, J. & Barckhausen, U. Evidence of low flexural rigidity and low viscosity lower continental crust during continental break-up in the South China Sea. *Mar. Pet. Geol.* **19,** 951–970 (2002).

22. Savva, D. *et al.* Different expressions of rifting on the South China Sea margins. *Mar. Pet. Geol.* **58,** 579–598 (2014).

23. Brune, S., Heine, C., Clift, P. D. & Pérez-Gussinyé, M. Rifted margin architecture and crustal rheology: Reviewing Iberia-Newfoundland, Central South Atlantic, and South China Sea. *Mar. Pet. Geol.* **79,** 257–281 (2017).

24. Whitmarsh, R. B., Manatschal, G. & Minshull, T. a. Evolution of magma-poor continental margins from rifting to seafloor spreading. *Nature* **413,** 150–4 (2001).
25. Minshull, T. A., Dean, S. M., White, R. S. & Whitmarsh, R. B. Anomalous melt production after continental break-up in the southern Iberia Abyssal Plain. *Geol. Soc. London, Spec. Publ.* **187,** 537–550 (2001).
26. Huismans, R. S. & Beaumont, C. Roles of lithospheric strain softening and heterogeneity in determining the geometry of rifts and continental margins. *Geol. Soc. London, Spec. Publ.* **282,** 111–138 (2007).
27. White, R. & McKenzie, D. Magmatism at rift zones: The generation of volcanic continental margins and flood basalts. *J. Geophys. Res.* **94,** 7685 (1989).
28. Geoffroy, L., Burov, E. B. & Werner, P. Volcanic passive margins: another way to break up continents. *Sci. Rep.* **5,** 14828 (2015).
29. Yu, C. *et al.* Deep thermal structure of Southeast Asia constrained by S-velocity data. *Mar. Geophys. Res.* **38,** 341–355 (2017).
30. Lizarralde, D., Gaherty, J. B., Collins, J. A., Hirth, G. & Kim, S. D. Spreading-rate dependence of melt extraction at mid-ocean ridges from mantle seismic refraction data. *Nature* **432,** 744–747 (2004).
31. Smith, W. H. & Sandwell, D. Global Sea Floor Topography from Satellite Altimetry and Ship Depth Soundings. *Science (80-.).* **277,** 1956–1962 (1997).
32. Wang, P., Prell, W. L. & Blum, P. *Proceedings of the Ocean Drilling Program, 184 Initial Reports*. **184,** (Ocean Drilling Program, 2000).
33. Sun, Z. *et al.* Proceedings of the International Ocean Discovery Program: Expeditions 367 and 368 scientific. (2018). doi:10.14379/iodp.proc.367368.2018
34. Seton, M. *et al.* Community infrastructure and repository for marine magnetic identifications. *Geochemistry, Geophys. Geosystems* **15,** 1629–1641 (2014).
35. Shervais, J. W. Ti-V plots and the petrogenesis of modern and ophiolitic lavas. *Earth Planet. Sci. Lett.* **59,** 101–118 (1982).

Author contributions

HCL.: Co-PI of the original drilling proposal, interpretation of seismic data, co-chief scientist of Exp 367/368, directed the writing of the paper

GM: Principal co-author, developed geodynamic model jointly with HCL and MN. Shipboard scientist (structural geology) at Exp. 368

MN: Shipboard scientist (structure/sedimentology) at Exp. 367. Structural interpretation of syn-rift sedimentation, contributed to model development and graphics

ZS: Co-PI of the original drilling proposal, interpretation of seismic data, co-chief scientist of Exp 367/368

JS: Co-chief scientist of Exp 367/368; co-proponent of original drilling proposal

ZJ: Co-chief scientist of Exp 367/368, coordinated biostratigraphic interpretations

AK: Expedition 367/368 project manager

CZ: Expedition 367/368 project manager and biostratigraphy

Expedition members:

Expedition 367 Scientists

Jacopo Boaga
Petrophysics

Anne Briais
Petrophysics

Yifeng Chen
Inorganic Geochemist

Michael J. Dorais
Inorganic Geochemist

Akira Furusawa
Paleontologist (foraminifers)

Jessica L. Hinojosa
Sedimentologist

Tobias W. Höfig

Petrologist

Kan-Hsi Hsiung
Sedimentologist

Baoqi Huang
Paleontologist (foraminifers)

Xiao-Long Huang
Petrologist

Benjamin G. Johnson
Sedimentologist

Chao Lei
Petrophysics

Li Li
Organic Geochemist

Zhifei Liu
Sedimentologist

Antonio Luna
Petrologist

Claudia Lupi
Paleontologist (nannofossils)

Anders J. McCarthy
Petrologist

Michael Nirrengarten
Structural Geologist

Caroline Robinson
Sedimentologist

Isabel Sauermilch
Petrophysics

Steven M. Skinner

Paleomagnetist

Xiang Su
Paleontologist (nannofossils)

Rong Xiang
Paleontologist (foraminifers)

Rajeev Yadav
Petrophysics

Liang Yi
Paleomagnetist

Cuimei Zhang
Structural Geologist

Jinchang Zhang
Petrophysics (

Yang Zhang
Paleomagnetist

Ning Zhao
Sedimentologist

Lifeng Zhong
Petrologist

Expedition 368 Scientists

Stephen A. Bowden
Organic Geochemist

Deniz Cukur
Petrophysics (

Kelsie A. Dadd
Sedimentologist

Weiwei Ding
Structural Geologist

Eric C. Ferré
Paleomagnetist

Fabricio Ferreira
Paleontologist (foraminifers)

Aaron J. Gewecke
Paleontologist (diatoms)

Enqing Huang
Petrophysics (Physical Properties) Specialist

Shijun Jiang
Paleontologist (nannofossils)

Haiyan Jin
Paleontologist (foraminifers)

Robert M. Kurzawski
Petrologist / Structural Geologist

Baohua Li
Paleontologist (foraminifers)

Yanping Li
Inorganic Geochemist

Jian Lin
Petrophysics

Chang Liu
Sedimentologist

Chuanlian Liu
Paleontologist (nannofossils)

Lachit Singh Ningthoujam
Petrophysics

Nobuaki Osono
Petrophysics

David W. Peate
Petrologist

Patricia Persaud
Petrophysics
ppersaud@lsu.edu

Ning Qiu
Petrophysics

Sara Satolli
Paleomagnetist

Julie C. Schindlbeck
Sedimentologist

Susanne M. Straub
Sedimentologist/Petrologist

Liyan Tian
Inorganic Geochemist

Froukje M. van der Zwan
Petrologist

Shiming Wan
Sedimentologist

Huaichun Wu
Paleomagnetist

Guangfa Zhong
Sedimentologist

Expedition 367/368 Scientists Addresses

c CAS Key Laboratory of Ocean and Marginal Sea Geology, South China Sea Institute of Oceanology, China
d Division of Geological and Planetary Sciences, California Institute of Technology, USA
e School of Ocean and Earth Science, Tongji University, 1239 Siping Road, Shanghai 200092, China
f International Ocean Discovery Program, Texas A&M University, 1000 Discovery Drive, College Station TX 77845, USA

610 g Dipartimento di Geologia Paleontologia e Geofisica, Università degli Studi di Padova, Italy,
611 h School of Geosciences, University of Aberdeen, Aberdeen, Scotland, United Kingdom, AB24
612 3UE.
613 i Observatoire Midi-Pyrenees, CNRS, France
614 j Guangzhou Institute of Geochemistry, Chinese Academy of Sciences, P.R. China
615 k Petroleum & Marine Research Division, Korea Institute of Geoscience and Mineral Resources
616 (KIGAM), 124 Gwahak-ro, Yuseong-gu, Daejeon 34132, Republic of Korea
617 l School of Geosciences, University of Sydney, NSW 2006, Australia
618 m Key Laboratory of Submarine Geoscience, Second Institute of Oceanography (SIO), State
619 Oceanic Administration (SOA), Baochubei Road 36, Hangzhou, China
620 n Department of Geology, Brigham Young University, USA
621 o Department of Geology, Southern Illinois University at Carbondale, 1259 Lincoln Drive,
622 Parkinson Lab, Carbondale IL 62901, USA
623 p Institute for Geosciences, Universidade Federal Fluminense (UFF), Brazil, CAPES Foundation,
624 Ministry of Education of Brazil, Brasilia - DF, Zip Code 70.040-020
625 q Department of Geoscience, Shimane University
626 r Earth and Atmospheric Sciences, University of Nebraska, Lincoln, 214 Bessey Hall, Lincoln NE
627 68588, USA
628 s JAMSTEC, Yokohama, Kanagawa 236-0001 Japan
629 t Department of Geology, Peking University, P.R China
630 u Guangzhou Institute of Geochemistry, Chinese Academy of Sciences, P.R China
631 v Institute of Groundwater and Earth Sciences, Jinan University, 601 West Huangpu Dadao,
632 Guangzhou GD 510632, China
633 w Geology and Geography, West Virginia University, USA
634 x GEOMAR Helmholtz Center for Ocean Research Kiel, Christian-Albrechts-Universität zu Kiel,
635 Wischhofstrasse 1-3, Kiel 24148, Germany
636 y Department of Marine Science and Engineering, China University of Geosciences, P.R. China
637 z Department of Micropalaeontology Nanjing Institute of Geology and Palaeontology, Nanjing,
638 P.R. China
639 aa School of Geographical and Oceanographical Sciences, Nanjing University, China
640 ab Department of Geology and Geophysics, Woods Hole Oceanographic Institution, 360 Woods
641 Hole Road, Woods Hole MA 02543, USA
642 ac Department of Geology and Geophysics, Louisiana State University, E235 Howe-Russell-
643 Kniffen, Geoscience complex, Baton Rouge LA 70803
644 ad Department of Geology, University of South Florida, Tampa, USA
645 ae Department of Earth and Environmental Sciences, Università degli studi di Pavia, Italy
646 af Institute of Earth Sciences, University of Lausanne, Switzerland
647 ag Department of Marine Geophysics, National Centre for Antarctic and Ocean Research
648 (NCAOR), Vasco Da Gama GOA 403804, India
649 ah Petrophysics(Physical Properties) Specialist, Faculty of Science, Graduate School of Science
650 and Technology for Innovation, 1677-1 Yoshida, Yamaguchi-shi,Yamaguchi 753-8512, Japan
651 ai Earth & Environmental Sciences, University of Iowa, 115 Trowbridge Hall, Iowa City IA 52242,
652 USA
653 aj School of Earth Sciences Ohio State Universit, USA

ak Department of Engineering and Geology, University of Chieti-Pescara, Via dei Vestini 31, Chieti Scalo 66013, Italy
al Institute of Marine and Antarctic Studies (IMAS), University of Tasmania, Australia
am Department of Geology, California State University, Sacramento, USA
an Lamont-Doherty Earth Observatory, Columbia University, 61 Route 9W, Palisades NY 10964, USA
ao Institute of Oceanography National Taiwan University, Tapei, Taiwan
ap Institute of Deep-sea Science and Engineering, Chinese Academy of Sciences, China
aq Institute of Geosciences, Christian Albrechts University Kiel, Ludwig-Meyn-Strasse 10, Kiel 24118, Germany
ar Institute of Oceanology, Chinese Academy of Sciences, 7 Nanhai Road, Qingdao Shandong Province 266071, China
as School of Ocean Sciences, China University of Geosciences, 29 Xueyuan Road, Haidian District, Beijing, China
at Department of Earth and Atmospheric Sciences, Purdue University, USA
au Institute of Oceanology Chinese Academy of Sciences, Guangzhou, P.R. China